Contents lists available at ScienceDirect

Catalysis Today

journal homepage: http://ees.elsevier.com

Effective photocatalytic degradation of Rhodamine B using tin semiconductors over hydrotalcite-type materials under sunlight driven

Sonia Mancipe [a,*], José J. Martínez [a], Cristian Pinzón [a], Hugo Rojas [a], Dora Solis [b], Ricardo Gómez [c]

[a] Escuela de Ciencias Químicas, Facultad de Ciencias. Universidad Pedagógica y Tecnológica de Colombia UPTC, Avenida Central del Norte, Tunja, Boyacá, Colombia
[b] Universidad Autónoma del Estado de México, Laboratorio de nanotecnología, Toluca de Lerdo, Mexico
[c] Universidad Autónoma Metropolitana, Laboratorio Eco-catálisis, Ciudad de México, Mexico

ARTICLE INFO

Keywords
Hydrotalcite-type materials
Tin semiconductors
Rhodamine B
Photodegradation
Charge carriers separation

ABSTRACT

In the current study, SnO_2(5, 10 and 15 wt%)/MgAl-HT hydrotalcite-type materials were synthesized by co-precipitation method. Besides, the photocatalytic activity of the materials was evaluated in the degradation of Rhodamine B under simulated sunlight. The characterization of the materials by X-ray diffraction (XRD), Raman spectroscopy, physisorption of nitrogen and X-ray photoelectron spectroscopy (XPS) showed the formation of the (003) and (110) characteristic plans of lamellar materials, vibrational modes typical of layered double hydroxides and tin, specific surface areas, pore size distribution and chemical composition, respectively. The photocatalytic activity showed that the SnO_2(10 %)/MgAl-HT catalyst has the best degradation of the dye reaching a 75 % of degradation after 210 min under simulated solar light irradiation. The route of action of charge carriers was evaluated using scavengers for photogenerated holes, hydroxyl and superoxide radicals, such as triethanolamine, isopropanol and benzoquinone, respectively, when benzoquinone was used it was confirmed that superoxide radicals play an important role in degradation of Rhodamine B.

1. Introduction

Wastewater from domestic and industrial sources contains a large amount of pollutants such as pesticides, detergents, drugs and dyes. These compounds can become harmful to the environmental and cause adverse health effects. Dyes are ionic salts solvated by water molecules making it difficult to separate them from water sources [1]. The Rhodamine B (RhB) is a dye that belong to the family of xanthenes that are often used in the staining industry and can also be used in biochemistry as a biology marker of viruses and diseases [2]. This highly stable molecule has been related with subcutaneous tissue sarcoma, irritation to eyes, skin and respiratory tract and suspected of being carcinogen and mutagenic for living organisms [3,4]. In addition, RhB can affect the photosynthesis of aquatic plants, since makes light absorption difficult [5]. Distinct techniques have been used for the treatment of pollutants such as dyes, which include different conventional treatment techniques as thermal degradation, biological treatment, adsorption and membrane separation treatment. However, biological treatments and adsorption require long operating times; thermal degradation consumes a large amount of energy. An alternative of treatment is the heterogeneous photocatalysis that is a radical-mediated oxidation process, capable of chemically modify the dyes, achieving a mineralization of the organic contaminants [6,7].

In this way, supported-semiconductor over mesoporous materials have demonstrated be adequate materials in the degradation of RhB [8], between those materials, the hydrotalcite- type materials or Layered Double Hydroxides (LDH) have emerged as promising photocatalysts due to their stable structure, high anion retention, charge separation and transfer efficiency, low-cost and facility of synthesis [9]. The hydrotalcite have a structure similar to brucite ($Mg(OH)_2$), where the magnesium atom is octahedrally coordinated to six hydroxyl groups [10]. When some divalent Mg atoms are isomorphically substituted by trivalent metals such as aluminum, a positive charge density is generated that is compensated by interlamellar anions such as carbonate anions [11]. The general formula of LDH is $(M_{1-x}^{II}M_x^{III}(OH)_2)A^{n-}{}_{x/n}\cdot mH_2O$ with M^{II} divalent metals, M^{III} trivalent metals and A^{n-} interlamellar anions, in the interlamellar regions there is also the presence of water molecules and hydroxyl ions [12].

However, the rate degradation of RhB in hydrotalcites is highly dependent of coordination of the active species of the semiconductor [13,14], as oxidant type used [15–17]. For example, Zn/M–NO_3-LDHs (M = Al, Fe, Ti, and Fe/Ti) displayed high to moderate activity under visible-light irradiation, being most active Ti^{4+} species than Fe^{3+} [14]. Additionally, it has been reported that Pt nanoparticles intercalated in ZnTi-layered double hydroxides favors the degradation of rhodamine due to high specific area, the negative shift in potentials and the easy

* Corresponding author.
E-mail address: sonia.mancipe@uptc.edu.co (S. Mancipe)

https://doi.org/10.1016/j.cattod.2020.12.014
Received 21 May 2020; Received in revised form 22 October 2020; Accepted 8 December 2020
Available online xxx
0920-5861/

of migration of photogenerated electrons that preventing recombination of the e^-/h^+ pair [18].

In particular, the use of hydrotalcite-type materials in the degradation of RhB result a catalyst depending of oxidant employed. For example, CoMgAl-LDHs is not as good photocatalyst in the degradation of this colorant using molecular oxygen [14], but, Cr-Zn layered hydroxide showed a degradation of rhodamine near to 100 %, employing H_2O_2. The formation $HO_2\cdot$ radicals resulting of the interaction between H_2O_2 and $HO\cdot$ is essential in the degradation of this colorant [17]. Thus same, cobalt phthalocyanine supported Mg–Al hydrotalcite using different H_2O_2 dosages reaches a degradation near to 90 % [19]. However, the effect of phtalocyanine was not discussed. Other efforts using this type of materials is the use of bicarbonate activated hydrogen peroxide to increase the degradation of Rhodamine [16].

On the other hand, the dispersion of n-type semiconductor in lamellar materials can favor the efficiency of the reaction of degradation of rhodamine. Tin oxide has been used in the dye degradation reactions, Babu and Antony employed SnO_2/bentonite nanocomposites in degradation of Methylene Blue (MB), in the photocatalytic mechanism suggest that electrons are excited to conduction band of SnO_2 and these electrons combined with oxygen lead to the formation of the superoxide radical ($O_2\cdot^-$), in this reaction they added hydrogen peroxide (H_2O_2), which favors the formation of hydroxyl radicals ($\cdot OH$), which are ultimately the species responsible for carrying out the degradation reaction [20]. Also, TiO_2 nanospheres over SnO_2 quantum dots composites were employed in the degradation of methyl orange, in this study SnO_2 quantum dots were dispersed over TiO_2 uniformly. In the discussion, Du and coworkers affirm that the efficiency in the photocatalytic activity using the composites is due to the synergistic effect between the two oxides [21].

If well, the role of semiconductor and the oxidant agent are indispensable in the degradation of RhB, the better results have been showed using typical semiconductors and H_2O_2 as a strong oxidant agent. In this work, we report the synthesis of materials of tin (IV) oxide over hydrotalcite-type materials used in the Rhodamine B photocatalytic degradation with simulated solar light. The advantage of this type of materials is the easy synthesis and the possibility of extend its use to scalable process using sunlight. It was also studied the role of some scavengers because of photogenerated charge carriers play an important role in the degradation of this type of colorants.

2. Experimental section

2.1. Synthesis of SnO_2/MgAl-HT

The solids SnO_2/MgAl with 5, 10 and 15 wt percent of tin oxide were synthetized by co-precipitation method. A mixture of the solutions of the precursor salts $Mg(NO_3)_2.6H_2O$ (0.43 mol) and $Al(NO_3)_3.9H_2O$ (0.14 mol) with a molar relation of 3 together with $SnCl_4.5H_2O$ were added to a three mouth-ball while maintaining constant agitation and room temperature. Afterwards, 2.61 mol of urea was added to the solution mixture and hydrolyzed at 373 K under reflux for 10 h. Additionally, the pH was adjusted with a $NaOH/Na_2CO_3$ solution 2 M until reaching a pH of 9.5. The resulting suspension was then kept at 433 K for 36 h. The precipitates were filtered and washed several times with deionized water. The samples were dried at 353 K and named as SnO_2(5%)/MgAl-HT, SnO_2(10 %)/MgAl-HT and SnO_2(15 %)/MgAl-HT. The SnO_2 content was determined by Energy-dispersive X-ray spectroscopy (EDS) and values were 5.11, 10.8 and 18.4 % for solids SnO_2(5%)/MgAl-HT, SnO_2(10 %)/MgAl-HT and SnO_2(15 %)/MgAl-HT, respectively, values which are closely to the theoretical ones. The MgAl-HT material was synthetized by co-precipitation method following the same methodology for SnO_2/MgAl-HT but without the presence of the of $SnCl_4.5H_2O$ semiconductor.

2.2. Characterization of the materials synthesized

The structure and crystallinity of the photocatalysts were measured by X-Ray diffraction using a Bruker D-2 Phaser diffractometer with CuKα irradiation in the range of 5° to 80°. The band gap energy of the photocatalysts were measured from the UV–vis spectra by extrapolating the reflectance to the X-axis for Y = 0, the Raman spectroscopy was realized using an HR LabRam 800 system equipped with an Olympus BX40 confocal microscope and a Nd: YAG laser beam (532 nm). The spectra were recollected in a cooled CCD camera with averaged for 100 accumulations in order to improve the signal to noise ratio, besides, all spectra were calibrated using the 521 cm^{-1} line of a silicon wafer. The textural properties of the materials were measured used a Quantachrome Autosorb 3B equipment, the samples were degassed out at 373 K by 16 h before the analysis. The XPS analysis were realized with a JEOL JPS-9200 instrument equipped with Mg Kα radiation source (1253.6 eV). The equipment was operated at an energy of 10 eV with an X-ray power of 300 W. The displacement for charge correction was done adjusting the spectrum with the 284 eV position of the carbon C (1 s). Deconvolution of each spectra was performed using Gaussian function of the Origin 8.1 software.

2.3. Photocatalytic activity

The photocatalytic activity test for the degradation of Rhodamine B (RhB), was performed using 25 mL of a 10 μM aqueous solution of the dye together with 12 mg of the photocatalysts added to a Petri dish. The first 30 min of reaction, the solution with the suspended material was allowed under stirring to ensure the adsorption-desorption equilibrium. Subsequently, the system was irradiated with a Sciencetech SF150 solar lamp equipped with an AM1.0D filter that simulated the sun´s spectrum. The solar simulator has a xenon lamp that emits with an intensity of 60 mW/cm^2 and it was kept at a distance of 15 cm from the surface. Aliquots were taken every 15 min during the first irradiation hour and after aliquots from reaction system were taken every 30 min until reaching 3 h of reaction time. The concentration of the organic molecule in this case Rhodamine B was followed through the UV–vis spectra in function of the reaction time, following the characteristic band of Rhodamine B peaking around 526 nm, using a Perkin Elmer Lambda 35 spectrophotometer. A photosensitization test was carried out using the material SnO_2(10 %)/MgAl-HT, the visible photocatalytic experiment was performed using an Osram Ultra-Vitalux lamp (300 W) and polyester UV filter sheet (Edmund Optics) showing 99.9 % of absorbance below 400 nm. The procedure of the activity under visible light irradiation was carried out in the same way as described above.

3. Results and discussion

3.1. Characterization of the materials

Fig. 1 shows the diffraction patterns of hydrotalcite-type materials and SnO_2. The characteristic peaks of lamellar solids (JCPDS 22–0700) corresponding to the basal plans (003), (006), (009), (015), (018) and (110) in angles 2θ at 11.59°, 23.32°, 34.77°, 39.37°, 46.8° and 64.64°, respectively [22], are present in MgAl-HT and SnO_2/MgAl-HT photocatalysts. The presence of the characteristic reflections in all the materials synthesized by co-precipitation method indicate that the formation of lamellar structure was effectively achieved despite the in-situ presence of the tin precursor. In the SnO_2/MgAl-HT solids it can be seen that with the increase of tin oxide on the support there is a decrease in crystallinity in the materials probably due to the fact that the segregated semiconductor generates a surface modification of MgAl-HT by the synthesis *in-situ* [23]. In addition, it can be seen that with the in-

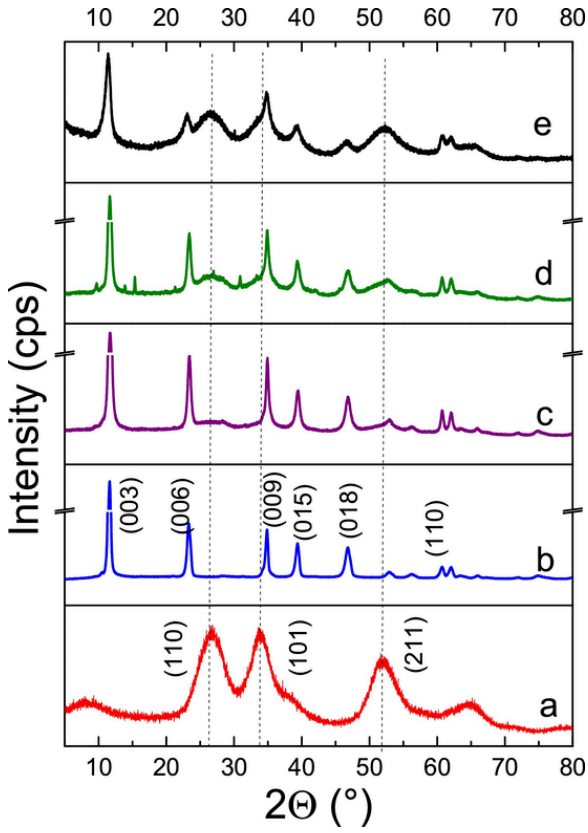

Fig. 1. X-ray diffraction patterns of a) SnO_2, b)MgAl-HT, c) SnO_2(5%)/MgAl-HT, d) SnO_2(10 %)/MgAl-HT, e) SnO_2(15 %)/MgAl-HT.

crease in the content of SnO_2 in the lamellar material, there is an increase in the signal at 26.54° in 2θ corresponding to the plane (110) of tin oxide showing the presence of the semiconductor on the surface. The reflections (110), (101) and (211) with JCPDS card N° 41–1445 [24] corroborate the presence of tin oxide in Fig. 1a.

The lattice parameters a (related to the distance between cations) and c (related with the interlamellar distance) [25] are shown in Table 1. As it can be seen, there is not significant variation in these parameters which assures that the layered structure is not modified. However, the presence of XRD signals of SnO_2 is indicative of its segregation on the surface of the hydrotalcite; i.e. the Sn was not introduced into the crystalline network of hydrotalcite because of ionic radius of Sn is higher compared with Al and Mg atoms. The crystallite size of SnO_2 measured in (110) plane does not show a greater variation with the increase in weight percentage, which may suggest that the presence of hydrotalcite prevents SnO_2 particle agglomeration [26].

On the other hand, the crystallite size of the hydrotalcite measured in the reflection (003) decreases in the SnO_2/MgAl-HT materials. The diminution in crystallite size is due to segregated particles of SnO_2 over the hydrotalcite surface causing a decrease in crystallinity, as can be seen in XRD. The addition of tin precursor during the coprecipitation of the magnesium and alumina salts modified the crystallite growth perturbing the reactions of hydrolysis-condensation induced by the presence of the urea and basic pH hindering the grown of MgAl particles [27]. This also affects the textural properties of the material (Fig S1). Thus an increase in surface area values was obtained with the incorporation of SnO_2. SnO_2/MgAl-HT 5 and 10 % solids showed the presence of meso-macroporosity. Taking in account the pore size distribution some changes in the meso and macroporous regions are observed as a function of the Mg content, which clearly shows developed microporosity in these samples that accounts for the increase of surface area which is more evident with a highest content of tin.

The band gap energy values calculated from the UV–vis diffuse reflectance spectra (no showed) are reported in the Table 1. It can be seen that with a high content of SnO_2 the band gap energy decrease from 5.10 eV for MgAl-HT to 3.80 eV for the SnO_2(15 %)/MgAl-HT. The increase in the intensity of absorption with the increase of tin oxide can be due to a greater absorption of photons by the material with 15 % of semiconductor. The decrease in the band gap energy with increase in the tin content would be related to the approach or approximation to the value the band gap of SnO_2 which is 3.68 eV [28].

Fig. 2 displays Raman spectra of the solids studied. In the spectrum the characteristic bands of the hydrotalcite-type materials are observed. The bands between 471 - 548 cm^{-1} are assigned to the linkage bonds as AlOAl and AlOMg of the hydrotalcite [29]. In this same region in the materials that containing SnO_2 appear bands around 474 cm^{-1} and 775 cm^{-1} which corresponding to the Eg and B_{2g} active Raman vibration mode, respectively for tin oxide [30]. On the other hand, the signal at 1060 cm^{-1} can be due to carbonate ions bonded to the brucite hydroxyl surface [29,31]. These signals increasing with the SnO_2 content evidencing that carbonate anions can be altered by the interaction with the hydroxyl groups or with water molecules that are also present in the interlamellar region [32]. The signal of low intensity around of 150 cm^{-1} can be assigned to deformation vibrations in M—OM— [33]. Previously Mancipe et al. [34], by UV–vis diffuse reflectance spectrum in this type of materials showed than Sn-O-Sn hexacordinated species are included over the lamellar structure [35]. An overtone of F2g around of 447 cm^{-1} and 493 cm^{-1} corresponding to Mg_2Sn can be observed [36].

Fig. 3a displays the high-resolution spectra of the region Sn $3d_{5/2}$. The deconvolution of the $Sn3d_{5/2}$ region showing two broad peaks. The line broadening in the spectrum also has been observed when is deposited SnO_2 in zeolites [37]. The first peak at 487 eV corresponds to Sn^{4+}. However, the second peak appears to lower values of BE (483 eV). Generally, the distance between peaks of Sn^{4+} and Sn^{2+} (486 eV) is associated with values near to 1.0, while the signal of Sn^0 appears generally to 484.6 eV [38]. Consequently, in the Sn/MgAl-HT materials is discarded the presence of Sn^{2+} or Sn^0. Therefore, we proposed that the peak to 483 eV is associated with Sn species negatively charged. Probably, the formation of Mg_2Sn could be responsible of this peak. In fact, the BE values near to 484 eV are assumed as Mg_2Sn [39–41]. The magnesium stannide (Mg_2Sn) charged negatively may be elec-

Table 1
Crystalline, spectroscopic and textural properties of MgAl and SnO_2/MgAl-HT photocatalysts.

Photocatalyst	Lattice parameters (nm)		Crystallite size (nm)		Band gap energy (eV)	S_{BET} (m^2/g)	
	a	c	SnO_2 D(110)	MgAl D(003)			Pore size distribution (nm)
MgAl-HT	0.3046	2.277	--	26.73	5.10	33	18
SnO_2(5%)/MgAl-HT	0.3046	2.276	2.16	19.53	4.05	87	35
SnO_2(10%)/MgAl-HT	0.3047	2.275	2.59	18.32	3.85	99	61
SnO_2(15%)/MgAl-HT	0.3049	2.274	2.61	13.00	3.80	111	24

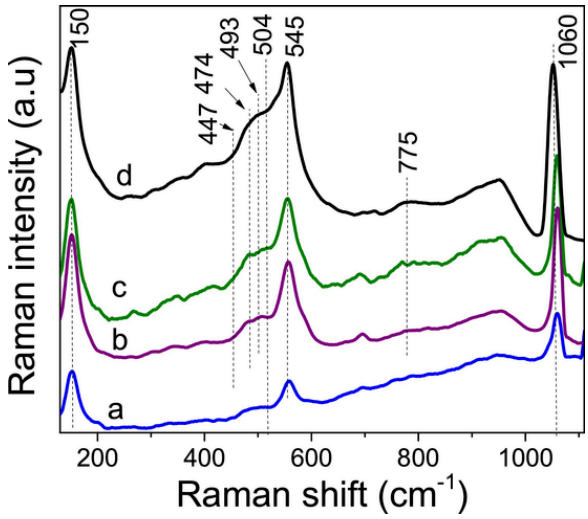

Fig. 2. Raman spectra of the materials a) MgAl-HT, b) SnO_2(5%)/MgAl-HT, c) SnO_2(10 %)/MgAl-HT, d) SnO_2(15 %)/MgAl-HT.

trostatically anchored to the charged positively hydrotalcite [42–45], this positive charge is formed when the divalent cation (M^{2+}) is isomorphically substituted by the trivalent cation (M^{3+}) [46]. The formation of Mg_2Sn are not was evidenced by DRX due to overlapping of the signals with the peaks characteristic of hydrotalcite-type materials.

On the other hand, in the high resolution spectrum of O 1s shows two peaks at 531.8 and 528 eV labelled as O_{II} and O_I. Typically, these peaks are related to oxygen vacancies and to lattice oxygen bonds, respectively [47]. The ratio between these two signals is showed in the Table 2. It can be observed that the incorporation of 5 % of SnO_2 in the surface of the hydrotalcite decreases the amount of O_I. However, with a higher incorporation of SnO_2 this value is increased. Clearly the solid SnO_2(10 %)/MgAl-HT possesses the highest ratio of tin species, while it maintains the oxygen vacancies on the surface of the hydrotalcite, as can be observed in the Table 2. The increase in tin content can lead to the formation of clusters, while with less tin it is possible to form layers, which could be in agreement with an increase in the oxygen vacancies in the catalyst with 5% and a decrease in the solid with 15 % of tin.

3.2. Photocatalytic activity

Fig. 4 shows the UV–vis spectra of the degradation of RhB using the SnO_2(10 %)/MgAl-HT catalyst with irradiation of the solar simulator and visible light, respectively. In the Fig. 4a the signal that was followed for the degradation of the dye is around 526 nm, in the spectra it can be observed that the absorbance decrease with reaction time. The maximum absorption shows that there is a slight hypsochromic shifts (526 nm to 524 nm) that may be the result of the formation of a series of N-de- ethylated intermediates [48]. After of 60 min of reaction the

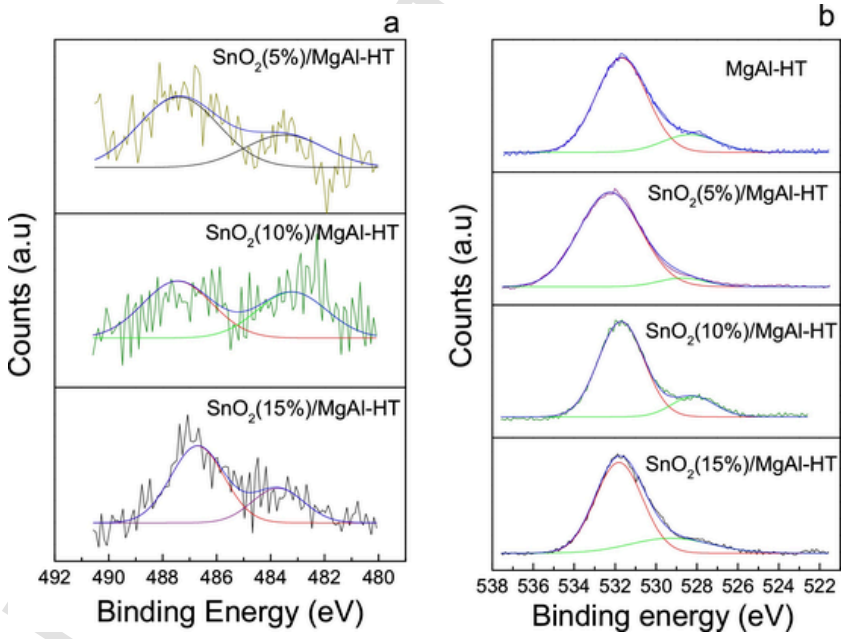

Fig. 3. High resolution spectra of a) Sn $3d_{5/2}$ and b) O1 s of photocatalysts.

Table 2
Atomic ratio obtained by XPS.

ratio	MgAl-HT	SnO_2(5%)/MgAl-HT	SnO_2(10%)/MgAl-HT	SnO_2(15%)/MgAl-HT
Mg/Al	1.4	0.9	1.7	2.2
Sn/Mg	---	0.01	0.01	0.04
O_{II}/O_I+O_{II}	0.85	0.95	0.85	0.77
O_I/O_I+O_{II}	0.15	0.05	0.15	0.33
Mg_2Sn/SnO_2+Mg_2Sn	--	0.2	0.5	0.3

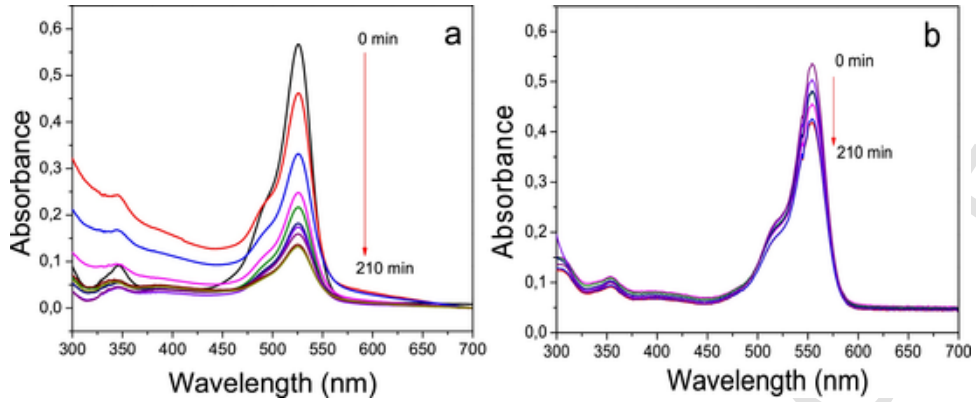

Fig. 4. UV–vis absorbance spectra of RhB dye degradation with SnO_2(10 %)/MgAl-HT with a) solar simulator and b) Visible light.

band at 345 nm decreased significantly, indicating that benzene-based intermediates similarly degrade to Rhodamine B [49].

In the Fig. 4b it can be observed a small decrease in the absorbance when SnO_2(10 %)/MgAl-HT is irradiated only with visible light, this diminution in the absorbance can be assigned to the formation of oxidant species from to the reactions of oxygen with the electrons transferred from HOMO to the LUMO in the Rhodamine B [50]. This behavior would be according with the photosensitizing effect of the dyes. However, it can be observed that when irradiating SnO_2(10 %)/MgAl-HT with only visible light the photocatalytic activity is low, this behavior could be due to the fact that the active phase is not activated in visible light in order to carry out the photocatalytic activity in the degradation of Rhodamine B.

The relationship of relative concentration vs reaction time of the catalysts is shown in Fig. 5a. The reaction of photolysis without presence of catalyst shown a low reduction in the relative concentration, reaching 30 % dye degradation (Fig. 5b). Similarly, the MgAl-HT support does not show a good activity in the degradation of the organic pollutant (45 % of degradation). However, when tin oxide is added to the MgAl-HT support, it is observed that there is an effect in the 30 min of adsorption of the dye and in the degradation reaction at the time the solution is irradiated with the simulated solar light. The solids with 5, 10 and 15 % of semiconductor reaching a 65 %, 75 % and 56 % of degradation, respectively.

The RhB dye and the semiconductor are irradiated with a solar light source for the photosensitization and formation of charge carriers (pair e^--h^+), respectively (ec. 1 and 2). The electron is excited to the conduction band, this charge carrier reacting with oxygen to the form the superoxide radicals (ec. 3), the superoxide radicals can react with the water molecule, electrons of CB of the semiconductor and protons to lead to the formation of hydroperoxyl radicals and H_2O_2 (ec. 4–6). Thus, H_2O_2 react with photogenerated electrons to form the hydroxyl radical (ec. 7). In the holes, the oxidation of water or hydroxyl ions occurs to generate hydroxyl radicals that induce the oxidation of the substrate in the holes or vacancies generated (ec. 8 and ec. 9). The degradation reaction competes either via holes or electrons (ec. 10) to finally the contaminant be transformed to carbon dioxide and water [14,51,52].

$$RhB + h\nu \rightarrow RhB^* \quad (1)$$

$$RhB^* + SC \rightarrow \cdot RhB^+ + SC\,(e^-_{BC}) \quad (2)$$

$$SC\,(e^-_{BC}) + O_{2ads} \rightarrow SC + O_2{\cdot}^- \quad (3)$$

$$O_2{\cdot}^- + H_2O \rightarrow HOO\cdot + OH\cdot \quad (4)$$

$$SC\,(e^-_{BC}) + O_2{\cdot}^- + 2H^+ \rightarrow H_2O_2 \text{ec. 5 } 2O_2{\cdot}^- + 2H^+ \rightarrow O_2 + H_2O_2 \quad (6)$$

$$H_2O_2 + SC\,(e^-_{BC}) \rightarrow \cdot OH + OH^- + SC \quad (7)$$

$$SC\,(h^+_{BV}) + H_2O_{ads} \rightarrow SC + \cdot OH_{ads} + H^+ \quad (8)$$

$$SC\,(h^+_{BV}) + OH^-_{ads} \rightarrow SC + \cdot OH_{ads} \quad (9)$$

$$\text{Organic compound } (\cdot RhB^+) + O_2{\cdot}^- \text{or } \cdot OH \rightarrow H_2O + CO_2 \quad (10)$$

The presence of the semiconductors p-type and n-type of Mg_2Sn and SnO_2, respectively, over the surface the hydrotalcite, favors the photocatalytic activity in the degradation of Rhodamine B dye, this because the presence of the semiconductors prevents the recombination of charge carriers, species responsible for carrying out the oxidation reaction in this case. The p-n heterostructures favor charge separation of electron-hole pair and improve the absorption of light [53]. Besides,

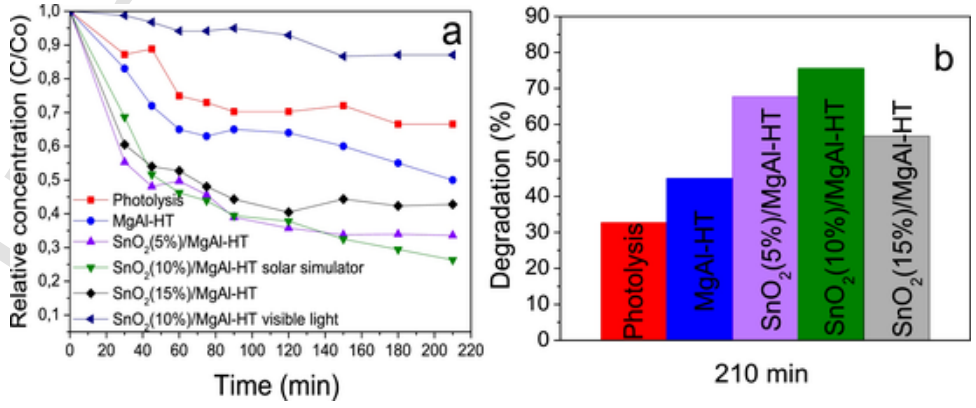

Fig. 5. Photocatalytic activity of RhB degradation a) relative concentration, and b) degradation percent with the synthesized materials.

according to the results shown in Fig. 5, the SnO_2(10 %)/MgAl-HT material exhibits the best photocatalytic activity, reaching 75 % degradation at 210 min of reaction. This behavior can be due to: i) the low crystallite size obtained in the plane (003) that possibly allows a better distribution of the active phase on the MgAl support, ii) a surface area greater than that presented in the hydrotalcite, iii) low recombination of the electron-hole pair formed after irradiation with simulated solar light, iv) higher $Mg_2Sn/SnO_2 + Mg_2Sn$ ratio shown by XPS and v) by the presence of meso/macroporosity that allows a better transport of reactants and products through the porous structure [54]. Besides, it should be noted that in these materials, a higher oxygen vacancy does not ensure that the activity increases as can be seen in Table 2, where O_{II} ratio is similar for MgAl-HT and SnO_2(10 %)/MgAl-HT

The degradation pathway of the contaminating molecule via electrons and holes photogenerated during the exposure of the reaction to solar light, was performed using scavengers, in similar way as it has been reported in the literature [55,56], with the purpose to identify the species responsible of the charge carriers which favors degradation. Isopropanol and triethanolamine were used separately, to evaluate the path of degradation by action of hydroxyl radicals (·OH) or photogenerated holes, respectively. On the other hand, benzoquinone was used to determine if the degradation route was carried out via the formation of supeoxide radicals ($O_2^{\cdot -}$) to lead to the obtaining ·OH radicals, which are finally the species that act on the contaminating organic matter [57]. The Fig. 6 shows the bar diagram of the relative concentration of RhB with each of the scavengers, using the photocatalysts SnO_2(10 %)/MgAl-HT.

With the addition of triethanolamine and isopropanol it is observed that there is degradation of the dye, however, when using benzoquinone, a scavenger for superoxide radicals, there is no degradation reaction. This behavior shows that the reaction takes place via photogenerated electrons.

In the representation showed in Fig. 7 it can be observed that the particles of p-n semiconductor are over the hydrotalcite surface, it can be observed that the p-n semiconductor are over the hydrotalcite surface, when the dye and semiconductors p-n are in contact and are irradiated with simulated solar light, exist transfer of electrons from HOMO to LUMO in the Rhodamine B, this electrons are transferred to CB of the semiconductor, the electrons are transfer from CB of p-type semiconductor (Mg_2Sn) to CB of n-type semiconductor (SnO_2) and holes are transfer to the Valence Band of the p-type semiconductors [58], favoring charge separation, agreeing to the results of activity it can be affirmed that the action of the electrons photogenerated by reaction with O_2, form the superoxide radicals which by successive reactions gives rise the hydroxyl radicals which may also be responsible for carried out the photo-degradation reaction of the dye.

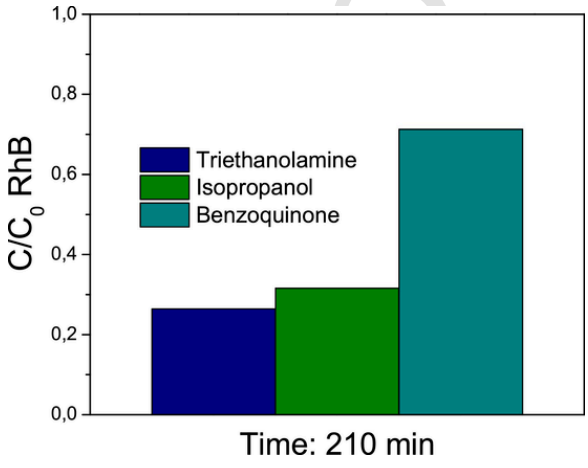

Fig. 6. Effect of scavengers on the degradation of Rhodamine B under simulated solar light irradiation using SnO_2(10 %)/MgAl-HT material.

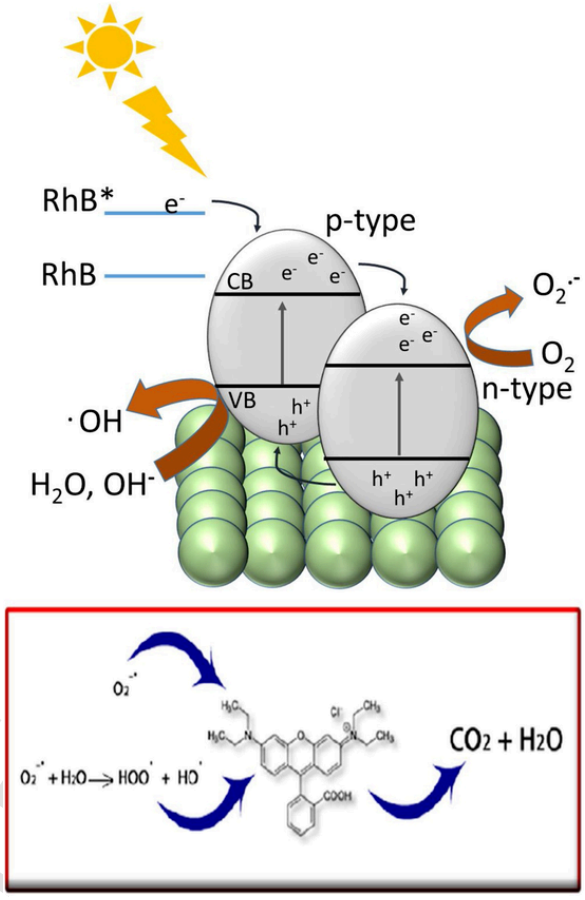

Fig. 7. Representation process of degradation of the RhB dye.

4. Conclusion

The synthesis of the hydrotalcite-type materials by co-precipitation method were successfully development. The characterization of the photocatalysts by XRD allowed demonstrating the formation of the laminar structure and the segregation of the SnO_2 particles on MgAl-HT. The pore size distribution indicates that the solid SnO_2(10 %)/ MgAl-HT presents a meso/macroporosity, which makes it an interesting material for the degradation reaction. The evaluation of the photocatalytic activity in the degradation of Rhodamine B showed that the material with 10 % semiconductor presents the best activity, due to the higher ratio $Mg_2Sn/SnO_2 + Mg_2Sn$ as has been showed by XPS, that favored the separation of the charge carriers. In addition, the evaluation using scavengers showed that the reaction occurs via the photogenerated electrons.

CRediT authorship contribution statement

Sonia Mancipe: Conceptualization, Methodology, Writing - original draft, Writing - review & editing, Project administration. **José J. Martínez:** Conceptualization, Methodology, Writing - original draft, Writing - review & editing, Supervision, Project administration. **Cristian Pinzón:** Writing - original draft, Writing - review & editing, Supervision. **Hugo Rojas:** Writing - review & editing, Project administration. **Dora Solis:** Writing - original draft, Writing - review & editing, Supervision. **Ricardo Gómez:** Conceptualization, Methodology, Writing - review & editing, Supervision.

Declaration of Competing Interest

The authors declare that they have no known competing financial interests or personal relationships that could have appeared to influence the work reported in this paper.

Acknowledgements

We acknowledgements to the CCIQS research center of UAEM-UNAM by X ray photoelectron spectra and the Nuclear Science Institute of the UNAM for the Raman analysis.

Appendix A. Supplementary data

Supplementary material related to this article can be found, in the online version, at doi:https://doi.org/10.1016/j.cattod.2020.12.014.

References

[1] L. Hossain, S.K. Sarker, M.S. Khan, Environ. Dev. 26 (2018) 23–33.
[2] F. Deng, Z. Xu, Chin. Chem. Lett. 30 (2019) 1667–1681.
[3] R. Jain, M. Mathur, S. Sikarwar, A. Mittal, J. Environ. Manage. 85 (2007) 956–964.
[4] T.K. Dixit, S. Sharma, A.S.K. Sinha, Inorg. Chem. Commun. 117 (2020) 107945.
[5] G. Utpal, P. Anjali, J. Photochem. Photobiol. A. (2020) 112582.
[6] M.Kaur Ritika, A. Umar, S.K. Mehta, S.K. Kansal, Mater. Res. Bull. 112 (2019) 376–383.
[7] A.P. Bhat, P.R. Gogate, J. Hazard. Mater. 403 (2021) 123657.
[8] S. Rasalingam, R. Peng, R.T. Koodali, Appl. Catal. B 174–175 (2015) 49–59.
[9] G. Zhang, X. Zhang, Y. Meng, G. Pan, Z. Ni, S. Xia, Chem. Eng. J. (2020) 123684.
[10] Z. Bouberka, K.A. Benabbou, A. Khenifi, U. Maschke, J. Photochem. Photobiol. A. 275 (2014) 21–29.
[11] G. Mishra, B. Dash, S. Pandey, Appl. Clay Sci. 153 (2018) 172–186.
[12] J.S. Valente, F. Tzompantzi, J. Prince, J.G.H. Cortez, R. Gomez, Appl. Catal. B 90 (2009) 330–338.
[13] N. Mao, Y. Jiao, ChemistrySelect 3 (2018) 12676–12681.
[14] S.-J. Xia, F.-X. Liu, Z.-M. Ni, J.-L. Xue, P.-P. Qian, J. Colloid Interface Sci. 405 (2013) 195–200.
[15] A. Auwalu, T. Linlin, S. Ahmad, Y. Hongying, J. Zhenan, Y. Song, Int. J. Ind. Chem. 10 (2019) 121–131.
[16] A. Jawad, X. Lu, Z. Chen, G. Yin, J. Phys. Chem. A 118 (2014) 10028–10035.
[17] N.T. Thao, H.T.P. Nga, N.Q. Vo, H.D.K. Nguyen, J. Sci. Adv. Mater. Devices 2 (2017) 317–325.
[18] G. Chen, S. Qian, X. Tu, X. Wei, J. Zou, L. Leng, S. Luo, Appl. Surf. Sci. 293 (2014) 345–351.
[19] M. Xu, Y. Cao, X. Ma, J. Nanosci. Nanotechnol. 16 (2016) 807–810.
[20] A.T. Babu, R. Antony, Appl. Clay Sci. 183 (2019) 105312.
[21] F. Du, X. Zuo, Q. Yang, B. Yang, G. Li, Z. Ding, M. Wu, Y. Ma, S. Jin, K. Zhu, Ceram. Int. 42 (2016) 12778–12782.
[22] H.M. Abdellattif, M. Mokhtar, Catalysts 8 (2018) 133.
[23] M. Intissar, F. Malherbe, V. Prévot, F. Leroux, J. Colloid Interface Sci. 299 (2006) 747–753.
[24] G. Ji, B. Ding, Z. Sha, J. Wu, Y. Ma, J.Y. Lee, Nanoscale 5 (2013) 5965–5972.
[25] Z. Yang, K.-M. Choi, N. Jiang, S.-E. Park, Bull. Korean Chem. Soc. 28 (2007) 11.
[26] H. Long, Y. Xu, X. Zhang, S. Hu, S. Shang, Y. Yin, X. Dai, J. Energy Chem. 22 (2013) 733–739.
[27] G. Mendoza-Damián, F. Tzompantzi, A. Mantilla, R. Pérez-Hernández, A. Hernández-Gordillo, Appl. Clay Sci. 121 (2016) 127–136.
[28] F.J. Arlinghaus, J. Phys. Chem. Solids 35 (1974) 931–935.
[29] S.J. Palmer, R.L. Frost, H.J. Spratt, J. Raman Spectrosc. 40 (2009) 1138–1143.
[30] I.M. Costa, Y.N. Colmenares, P.S. Pizani, E.R. Leite, A.J. Chiquito, Chem. Phys. Lett. 695 (2018) 125–130.
[31] R. Frost, W. Martens, K. Erickson, J. Therm. Anal. Calorim. 82 (2005).
[32] M. Mora, C. Jiménez-Sanchidrián, J. Rafael Ruiz, Mater. Lett. 120 (2014) 193–195.
[33] S. Paikaray, M.J. Hendry, Appl. Surf. Sci. 263 (2012) 633–639.
[34] S. Mancipe, F. Tzompantzi, H. Rojas, R. Gómez, Appl. Clay Sci. 129 (2016) 71–78.
[35] E. Dvininov, M. Ignat, P. Barvinschi, M.A. Smithers, E. Popovici, J. Hazard. Mater. 177 (2010) 150–158.
[36] L. Laughman, L.W. Davis, Solid State Commun. 9 (1971) 497–500.
[37] J.A. Jennings, S. Parkin, E. Munson, S.P. Delaney, J.L. Calahan, M. Isaacs, K. Hong, M. Crocker, RSC Adv. 7 (2017) 25987–25997.
[38] A. Nikiforov, V. Timofeev, V. Mashanov, I. Azarov, I. Loshkarev, V. Volodin, D. Gulyaev, I. Chetyrin, I. Korolkov, Appl. Surf. Sci. 512 (2020) 145735.
[39] D.-T. Nguyen, S.-W. Song, J. Power Sources 368 (2017) 11–17.
[40] D.-T. Nguyen, X.M. Tran, J. Kang, S.-W. Song, ChemElectroChem 3 (2016) 1813–1819.
[41] P. Claus, F. Raif, S. Cavet, S. Demirel-Gülen, J. Radnik, M. Schreyer, T. Fässler, Catal. Commun. 7 (2006) 618–622.
[42] S. Nayak, K.M. Parida, Sci. Rep. 9 (2019) 2458.
[43] Q. Li, C. Lu, C. Chen, L. Xie, Y. Liu, Y. Li, Q. Kong, H. Wang, Energy Stor. Mater. 8 (2017) 59–67.
[44] X. Ji, W. Zhang, L. Shan, Y. Tian, J. Liu, Sci. Rep. 5 (2015) 18367.
[45] Z. Wu, D. Khalafallah, C. Teng, X. Wang, Q. Zou, J. Chen, M. Zhi, Z. Hong, J. Alloys Compd. 1 (2020) 155604.
[46] M.S. San Román, M.J. Holgado, C. Jaubertie, V. Rives, Solid State Sci. 10 (2008) 1333–1341.
[47] L. Wang, X. Gao, Y. Cheng, X. Zhang, G. Wang, Q. Zhang, J. Su, J. Photochem. Photobiol. A. 369 (2019) 44–53.
[48] Z. He, C. Sun, S. Yang, Y. Ding, H. He, Z. Wang, J. Hazard. Mater. 162 (2009) 1477–1486.
[49] D.C. Khandekar, A.R. Bhattacharyya, R. Bandyopadhyaya, J. Environ. Chem. Eng. 7 (2019) 103433.
[50] D.A. Jennyfer, G.B. Islen, J.T. Christian, M. Miguel, P. Maria, M. Fiderman, Photochem. Photobiol. Sci. 18 (2019) 897–904.
[51] A.M. Al-Hamdi, U. Rinner, M. Sillanpää, Process Saf. Environ. Prot. 107 (2017) 190–205.
[52] W. Zhao, C. Chen, X. Li, J. Zhao, H. Hidaka, N. Serpone, J. Phys. Chem. B 106 (2002) 5022–5028.
[53] J. Xiong, H.-Y. Zeng, C.-R. Chen, G.-F. Xiao, D.-S. An, J. Alloys Compo. 833 (2020) 154898.
[54] M.I. Espitia-Cabrera, M.E. Contreras-García, M.L. García-Benjume, Int. J. Photoenergy. 2012 (2012) 1–10.
[55] D.P. Ojha, H.P. Karki, J.H. Song, H.J. Kim, Compos Part B-Eng. 160 (2019) 277–284.
[56] S. Zhou, N. Bao, Q. Zhang, X. Jie, Y. Jin, Appl. Surf. Sci. 471 (2019) 96–107.
[57] T.H. Huy, D.P. Bui, F. Kang, Y.-F. Wang, S.-H. Liu, C.M. Thi, S.-J. You, G.-M. Chang, V.V. Pham, Chemosphere 215 (2019) 323–332.
[58] H. Wang, L. Zhang, Z. Chen, J. Hu, S. Li, Z. Wang, J. Liu, X. Wang, Chem. Soc. Rev. 43 (2014) 5234–5244.